TECHNICAL PAPER

CrossMark

Analysis of the heat transfer coefficients of the whole process of continuous casting of carbon steel

Tarquínio Plynio Durães dos Anjos[1] · Paulo Vicente de Cassia Lima Pimenta[1] · Francisco Marcondes[1]

Abstract

In this work, we use a numerical–experimental approach which is based on the solution of the inverse heat conduction problem (IHCP) and temperature measurements. To obtain the profile of the heat transfer coefficients for all stages of the industrial manufacture of continuous casting process, we evaluate the three cooling regions. At primary ones, we use the temperature measured at the wall of the mold by thermocouples and the surface temperature of the ingot in the secondary and tertiary regions by optical pyrometers placed at the strategic positions. The IHCP procedure analysis the behavior of the numerical heat transfer coefficient under several conditions, such as casting temperature and speed as well as the chemical composition of the steel. We also propose a correlation to evaluate the overall heat transfer coefficient profile as function of the investigated parameters.

Keywords Continuous casting · Heat transfer coefficient · Numerical–experimental approach · Ingot solidification

1 Introduction

Continuous casting is currently the most used technique in the world for the production of semi-finished steel and alloy goods. This process basically consists of the continuum solidification of alloys of steel, aluminum, or copper, resulting in a product with a shape of a billet, plate, or block [1, 2]. During the solidification process, in the cast machine, the ingot is subject in general to three cooling zones which are called: primary, secondary and tertiary regions. The primary region corresponds to the mold, which is water-cooled. This step is responsible for the formation of a thin metal shell, which must be able to prevent breakout due the ferrostatic pressure. At the secondary stage, the ingot is cooled by the water-cooled sprays. The final solidification step is at tertiary region, in which the ingot is cooled by radiation and natural convection. Since it was introduced in the industry, the continuous casting technique has been improved to prevent the formation of defects and hence reduce the costs and production time [1, 3]. Therefore, the operational steps must be carefully controlled to ensure stable, uninterrupted, and reproducible procedures [3]. Clearly, various complex physical elements are present in the operational process, such as transient effects (turbulence, argon injection, and superheat removal), periodic oscillations of the mold, ingot contraction at the mold region, contact with the rolls, casting speed, chemical composition, and the phase change [4–9].

However, the main physical phenomena source that affects the continuous casting is the heat transfer in all three regions. For instance, irregularities in the cooling process at the boundaries of the mold may induce an uneven solid ingot shell, which can produce breakpoints at the mold exit or crack formation [1, 5, 8, 10, 11]. These problems directly influence the quality and cost of production. Thus, the knowledge of the heat flow mechanism can provide important information to improve the industrial process [1, 10].

The volumetric shrinkage associated with the expansion caused by the metallostatic pressure during solidification can even cause irregularities in the solid shell formation. These factors can lead to grips and/or depressions of the ingot in the mold region. Wolf [12] performed

---

Technical Editor: Francis HR Franca.

✉ Francisco Marcondes
 pimenta.pvcl@gmail.com

[1] Department of Metallurgical Engineering and Material Science, Federal University of Ceará Campus do Pici, Bloco 729, Fortaleza, Ceará 60455-760, Brazil

solidification tests and developed a technique for estimating the potential tendency for depression and grip formation in continuous casting of the carbon steel alloys in mold region. The methodology involves the ferritic potential (FP), which indicates the solid fraction of ferrite according to the carbon equivalent concentration C_{eq}(wt%).

Wolf also defined the following terms: steel type A with $0.85 \leq FP \leq 1.05$, which exhibits tendency to form depression, and steel type B with $FP > 1.05$ or $FP < 0.85$, which has tendency to grip at the walls of the mold.

The knowledge of the heat flow mechanism can provide important information to improve the solidification process [1, 10]. In the literature, we can find numerous works with different approaches, which focus on the investigation of the heat transfer in continuous casting of steel. These methodologies can be divided into analytical [13, 14] and numerical–experimental [10, 15] procedures. It is worth noting that the numerical–experimental schemes have been received more attention. One of this application can be found in the work of Barcellos et al. [10], which apply a methodology that involves the solution of the Inverse Heat Conduction Problem (IHCP), in conjunction with the Finite Difference Method (FDM), to evaluate the heat transfer coefficient in the metal/mold interface. They also investigated the effect of the metal mold interface coefficient under different casting parameters, as casting speed, chemical composition, and geometry of the mold. Cheung et al. [15] also studied the interface coefficient at the mold. In this work, they introduced a technique that uses FDM and an artificial intelligence heuristic search method, which is able to choose the suitable heat transfer coefficient to optimize the cooling conditions and avoid defect formation in the billet production. Nevertheless, when it comes to investigation of heat transfer coefficient in continuous casting, most studies focus only at the mold region.

We propose an approach to evaluate the heat transfer coefficient for the whole continuous casting of steel process in terms of chemical composition, which is presented as a function of FP, casting temperature, and speed. These results can be used as background information in numerical experiments, which analyses ideal parameters during solidification process. The solution of the inverse heat conduction problem (IHCP) using a Finite Volume Method (FVM) and experimental temperature measurements data are able to make a complete physical description of the heat transfer coefficient behavior. More details about IHCP approach can be found in [10, 16–21].

The FVM is a conservative approach at the discrete-finite-volume level [22, 23]. It is also important to point out that the FVM has been applied to several areas, as for instance, in structural analyses [24–26], computational fluid dynamics [27] and fluid–structure iteration [28].

2 Physical model

The main propose of this section is to define the procedure adopted to analyze the interfacial metal/mold heat transfer coefficient at the inner, outer and side face of the mold region. The domain and boundary condition is illustrated in the Fig. 1a. A unidimensional model was adopted, since this is a simplistic and a very effective way to evaluate these heat transfer coefficients.

The unidimensional heat equation with a source term, q which is related to the phase change, might be expressed as:

$$\frac{\partial}{\partial t}(\rho c T) = \frac{\partial}{\partial x}\left(k\frac{\partial T}{\partial x}\right) + q, \tag{1}$$

where ρ (kg m^{-3}) is the density, c (J kg^{-1} K^{-1}) denotes the specific heat capacity, κ (W m^{-1} K^{-1}) is the thermal conductivity, t (s) is the physical time, and T (K) stands for the temperature. The source term in Eq. (1) is given by:

$$\dot{q} = \rho L\left(\frac{\partial f_s}{\partial T}\frac{\partial T}{\partial t}\right), \tag{2}$$

where f_s is the solid fraction and L (J kg^{-1}) is the latent heat. Substituting Eq. (2) into Eq. (1) and using the concept of apparent specific heat (c'), $c' = c - L\left(\frac{\partial f_s}{\partial T}\right)$, we can rewrite Eq. (1) as:

$$\frac{\partial}{\partial t}(\rho c' T) = \frac{\partial}{\partial x}\left(\kappa\frac{\partial T}{\partial x}\right). \tag{3}$$

The solid fraction, f_s, depends on several factors such as alloy constituents as well as the diffusion during solidification. However, in this work, we assume the expression described in Garcia [29], which f_s depends only on the temperature, and it can be expressed by:
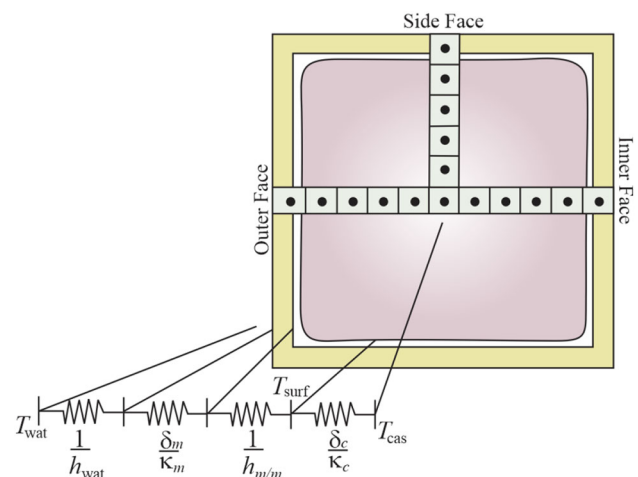

Fig. 1 Cross section of ingot mold. Schematic of the grid in vertical plane and the thermal resistances

$$f_s = \left(\frac{1}{1-k_0}\right)\left(\frac{T_L - T}{T_F - T}\right), \tag{4}$$

and

$$\frac{\partial f_s}{\partial T} = \left(\frac{1}{1-K_0}\right)\left(\frac{T_L - T}{(T_F - T)^2} - \frac{1}{T_F - T}\right), \tag{5}$$

where K_0 is the partition coefficient, where it was assumed to be constant and equal to 0.2 (carbon steel). T_F is the solvent melting temperature (iron), and T_L is the liquidus temperature, which is given by:

$$\begin{aligned}T_L(°C) = {}& 1537 - 88\%C - 8\%Si - 5\%Mn - 30\%P \\ & - 25\%S - 5\%Cu - 4\%Ni - 1.5\%Cr - 2\%Mo \\ & - 2\%V - 24\%As - 18\%Ti.\end{aligned} \tag{6}$$

The steel composition and thermophysical properties used in this work are shown in Table 1. The material properties are defined in terms of the solid fraction, according to the following relationships:

$$\begin{aligned} c &= f_s c_s + (1 - f_s)c_l, \\ \kappa &= f_s k_s + (1 - f_s)\kappa_l, \\ \rho &= f_s \rho_s + (1 - f_s)\rho_l, \end{aligned} \tag{7}$$

where the subscripts s and l represent the properties of the solid and liquid phases, respectively.

The convective effect present in the liquid pool is not considered in the current approach. Therefore, we replace the thermal liquid conductivity (κ_l) by an effective thermal conductivity, κ_{efe}, whose value is in the range of 5–10 times greater than the thermal coefficient of liquid material phase.

$$\kappa_{efe} = A\kappa_l, \tag{8}$$

where $5 \le A \le 10$. In this work, we adopted $A = 7$.

Using the finite volume method (FVM) in and explicit time integration, we obtain the following linear equation:

$$\frac{\rho c'T|_i^{n+1} - \rho c'T|_i^n}{\Delta t}\Delta x = \left.\frac{k}{\Delta x}\right|_{ip1} T_{i-1}^n + \left.\frac{k}{\Delta x}\right|_{ip2} T_{i+1}^n \\ - \left(\left.\frac{k}{\Delta x}\right|_{ip1} + \left.\frac{k}{\Delta x}\right|_{ip2}\right) T_i^n, \tag{9}$$

where i denotes the control-volume and $i-1$ and $i+1$ denote its neighbors, n and $n+1$ refers to the previous and current time-step, respectively, $ip1$ and $ip2$ correspond to the interfaces of control-volume i. It is convenient to reorganize Eq. (9) as:

$$T_i^{n+1} = \frac{\Delta t}{\rho_i c_i' \Delta x A}\left.\frac{Ak}{\Delta x}\right|_{ip1} T_{i-1}^n + \frac{\Delta t}{\rho_i c_i' \Delta x A}\left.\frac{Ak}{\Delta x}\right|_{ip2} T_{i+1}^n \\ - \frac{\Delta t}{\rho_i c_i' \Delta x A}\left[\left(\left.\frac{Ak}{\Delta x}\right|_{ip1} + \left.\frac{Ak}{\Delta x}\right|_{ip2}\right) - 1\right] T_i^n. \tag{10}$$

In the above equation, the thermal conductivity at each integration point might be expressed in terms of the inverse of the thermal resistance R (see Fig. 1), which leads to [10, 30]:

$$T_i^{n+1} = \frac{\Delta t}{C}\left(\frac{T_{i-1}^n}{R_{i-1} + R_i} + \frac{T_{i+1}^n}{R_{i+1} + R_i}\right) \\ - \frac{\Delta t}{C}\left[\left(\frac{1}{R_{i-1} + R_i} + \frac{1}{R_{i+1} + R_i}\right) - 1\right] T_i^n, \tag{11}$$

where C (J K^{-1}) represents the accumulated energy [10] in a volume element i, R stands for thermal resistances evaluated at the control-volume i and its neighbors $i-1$ and $i+1$. The accumulated energy can be expressed as:

$$C = \rho_i c_i' \Delta x, \tag{12}$$

and resistances is written by:

$$R_{i-1} = \frac{\Delta x_{i-1}}{2\kappa_{i-1}}, \tag{13a}$$

$$R_i = \frac{\Delta x_i}{2\kappa_i}, \tag{13b}$$

Table 1 Thermophysical properties of metal and mold

Property	Value			
	Metal			Mold
	1013D	1034D	1028D	
Liquidus thermal conductivity κ_l (W m^{-1} K^{-1})	35	34.7	29	340
Solidus thermal conductivity κ_s (W m^{-1} K^{-1})	35.5	31	30	
Liquidus heat capacity c_l (J kg^{-1} K^{-1})	674	600	600	
Solidus heat capacity c_s (J kg^{-1} K^{-1})	688	640	642	386
	7000	7000	7000	
Liquidus density ρ_l (kg m^{-3})	7490	7290	7850	8900
Solidus density ρ_s (kg m^{-3})				
Latent heat L (J kg^{-1})	273,000	245,000	277,000	

$$R_{i+1} = \frac{\Delta x_{i+1}}{2\kappa_{i+1}}. \tag{13c}$$

The numerical domain presents four boundary conditions (see Fig. 1), which must be carefully evaluated at following regions: interface mold/environment, interface metal/mold, and inside of the mold (at the center). For the control-volumes in contact with the walls of the mold (see Fig. 1), the thermal resistance is given by:

$$R_{\text{wall}} = \frac{1}{h_{\text{m/m}}}, \tag{13d}$$

where $h_{\text{m/m}}$ (W m^{-2} K^{-1}) is the metal/mold heat transfer coefficient (Fig. 1). This coefficient represents the thermal resistance due to the gap or grip between the mold and metal. Further details about the physical model can be found in [10, 15, 30].

The approach to obtain the heat transfer coefficients at the metal/mold interfaces (inner, outer, and side faces) used in this work is similar to the one used by Barcellos et al. [10], which applied the FDM as the numerical approach. The boundary conditions were applied to the one-dimensional grid, as shown in Fig. 1. The temperatures of the water, T_{wat}, the casting, T_{cas}, and the heat transfer coefficient for the cooling water, $h_{\text{wat}}(h_{\text{wat}} = 24,528\ \text{Wm}^{-2}\text{K}^{-1})$ [31], were considered constant along all the length of the mold. The grid moves with the same speed of the continuous casting.

After the mold, the analyses of the heat transfer coefficients take place at the sprays section. This stage ensures the continued development of the solidified shell. In general, the secondary region is divided in three sub-zones according to the water flow rate. As the surface temperature of the ingot decreases, the flow rate and the number of sprays per zone also decrease, since the thermal resistance of the liquid steel heat transfer to the environment increases. Empirical formulations have been developed to relate the heat transfer coefficient at the spray region according to various parameters, such as type of nozzles, pressure and water flow rate, nozzle distance from the ingot, and the water temperature [32]. For the heat transfer coefficient at the spray region, we assumed that the heat transfer coefficient is dependent on the water flow rate, m, as proposed by Brimacombe et al. [33], which can be expressed by:

$$h_{\text{sprays}} = 0.366\ m^n, \tag{14}$$

where n is a constant which must be adjusted with the aid of IHCP. The heat transfer coefficients for the secondary and tertiary regions are presented in the results' section.

3 Numerical–experimental methodology

In the numerical experiments, we use a mesh with 1532 volumes, which was enough to ensure grid independently results. The time-step is chosen using the following expression:

$$\Delta t > \frac{\Delta x}{2\kappa}\rho c', \tag{15}$$

which prevent instabilities in the explicit formulation employed.

For the experimental procedure, in the mold region, fifteen K Chromel–Alumel thermocouples, with diameter of 1.5 mm, were inserted at specific positions (see Fig. 2) in each three walls of the mold (inner, outer, and lateral). To reduce the possibility of deformation, the thermocouples were fixed in a 4 mm depth from the cold surface of the mold. To obtain the flux along the three faces, five thermocouples were positioned equally spaced on each face. The first three thermocouples were positioned closer to the meniscus, where larger heat transfer coefficients are expected. Figure 2a shows the lateral of the mold with the grooves where the thermocouples were inserted, and Fig. 2b shows the view of the top of a cross section of the mold.

With the purpose of evaluating the $h_{\text{m/m}}$, a one-dimensional approach over a half ingot plus mold cross section was applied, as it is shown in Fig. 1. Water temperature was considered constant along all the length of the mold, and the casting temperature was measured by an immersion thermocouple tip before each process. The methodology for obtaining the heat transfer coefficient at each metal/mold interface consists of using the inverse solution of heat conduction equation (IHCP). The process starts by assuming a heat transfer coefficient between the ingot and mold interface equal to zero, and then the temperature field
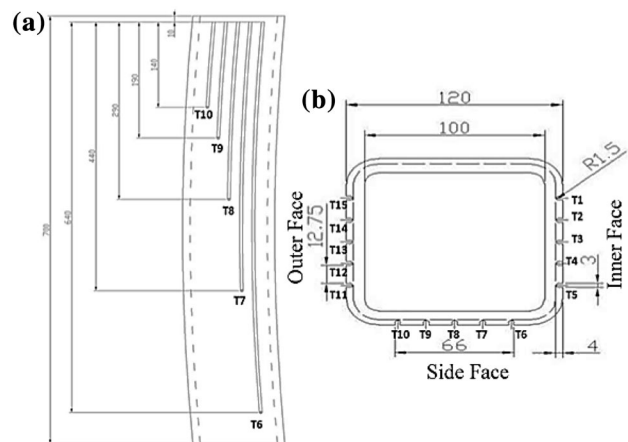

Fig. 2 Thermocouple distribution scheme. **a** Lateral of the mold, **b** cross-section of the mold

from the center of the ingot to the water is evaluated. Therefore, we compare the measured temperature with the calculated temperature. If the difference between the values does not satisfy the tolerance ($\pm$ 1 °C), the coefficient $h_{m/m}$ is updated by a $\Delta h_{m/m}$ factor, which in our experiments was chosen as $10^{-6}\mathrm{Wm}^{-2}\mathrm{K}^{-1}$. Thereby, when the algorithm finds one $h_{m/m}$ which satisfies the tolerance, the procedure moves to the next thermocouple at the point $\Delta t v_{cas}$, where v_{cas} is the casting speed, assuming the value previous calculated as the initial guess. The heat transfer coefficient does not change until the next thermocouple is found, when the previous process is repeated to evaluate a new heat transfer coefficient. It is worthwhile to mention that the tolerance temperature of the $\pm$ 1 °C was chosen after some numerical tests, which show that this is the minimal value which was able to make the process efficient without compromise the numerical results. A similar approach can be found in [1, 6, 10, 15].

A similar approach used in the mold region is used to evaluate the heat transfer coefficient to the secondary and tertiary regions, but now we measure the temperature of the surface of the ingot using an optical pyrometer. The numerical–experimental procedure for the sprays section, Eq. (14), is used to evaluate the exponent n, resulting in $n = 0.56$ for the 1028D and 1034D steels and $n = 0.63$ for the 1013D steel, similar results were found by Bolle and Moureau [32].

For the region of cooling by radiation/natural convection, the heat transfer coefficient is guessed using the value previous calculated at the end of the secondary region and its value is further adjusted with the temperature measured with the optical pyrometer (RAYTEK 23131). Once the heat transfer coefficient is calculated it does not change. This procedure was manually executed at fifteen defined points.

4 Results

The experimental data were obtained by monitoring 75 continuous casting of steel with the average duration of 45 min. At the primary cooling zone, the thermal measurements were monitored by a software and stored at each minute for posterior treatment. At the secondary and tertiary zones, the temperature measurements were taking manually with the use of the optical pyrometer (RAYTEK 23131). For this region, we chosen several fixed points in which fifteen measures were made; the surface temperature of the ingot was taken as the average of these measurements.

4.1 Analysis of the heat transfer coefficient in the mold region

The experimental data was obtained by monitoring 75 continuous steel casting processes with the average duration of 45 min. The chemical composition and the casting parameters process are shown in Table 2, where T_{cas} stands for the casting temperature.

From the experimental data and the IHCP, the effects of chemical composition, represented by ferritic potential (FP) on the heat transfer coefficient $h_{m/m}$, are shown in Fig. 3 for all the investigated surfaces of the mold. These results point out that the highest values of heat transfer coefficient are for those steels that have the high carbon concentration (C_{eq}), i.e., by increasing the ferritic potential, the coefficient decreases. Such behavior can also indicate the tendency of increasing the gap for type A, as well as gripping for type B steels, between the ingot and walls of the mold. The results show also, for both steels grades, that the greatest heat transfer values lie in the meniscus region and decreases along the mold length. Similar results can be found in [10, 34–36].

The heat transfer coefficients at the three investigated surfaces (inner, outer, and lateral) for A and B steels are shown in Fig. 4.

In Figs. 3 and 4, it is possible to observe the heat transfer at the side face has the lowest value. We also observed the heat transfer coefficient profile at the outer face, for both A and B steel types, has the highest relative value except at the mold exit. This result can be explained by the higher contact between the ingot and the outer face of the mold due to action of the weight of the ingot combined with its bending. At the bottom of the mold, the ingot has suffered considerable contraction, hence increasing the gap between the ingot and mold with consequent increase of the thermal resistance.

The effect of casting speed on the heat transfer coefficient for steels A and B at the metal/mold interface for operating casting speed range (2.70–3.40 m/min) are shown in Figs. 5 and 6.

In Figs. 5 and 6, we can see that casting speed directly influences the heat flux for each type of steel. As the casting speed increases, the heat transfer coefficient becomes greater mostly next to the meniscus. According to de Barcellos et al. [10] and Chow et al. [37], such behavior is due to the three following main reasons: Firstly, high-speed results in a thinner solidified shell, which under action of the ferrostatic pressure deform easily, and therefore reduces the gap at each metal/mold interface. Secondly, the surface of the ingot will become hotter, which will increase the thermal gradient and hence the heat

Table 2 Chemical composition and casting parameters

| Steel	Chemical composition (%)														T_L (°C)	T_{cas} (°C)	v_{cas} (m min^{-1})
	C	Mn	Si	S	P	Cu	Cr	Ni	Mo	As	Nb	Sn	V	Al			
1013D	0.07	0.45	0.15	0.0	0.0	0.0	0.0	0.0	0.0	0.0	0.0	0.0	0.0	0.0	1528	1540–1560	2.7–3.2
	0.15	0.70	0.30	0.036	0.04	0.35	0.35	0.35	0.05	0.05	0.015	0.09	0.015	0.1	1512		
1028D	0.25	0.5	0.15	0.0	0.0	0.0	0.0	0.0	0.0	0.0	0.0	0.0	0.0	0.0	1511	1520–1540	
	0.3	0.7	0.3	0.036	0.06	0.35	0.25	0.25	0.05	0.05	0.015	0.09	0.015	0.1	1498		
1034D	0.3	0.5	0.15	0.0	0.0	0.0	0.0	0.0	0.0	0.0	0.0	0.0	0.0	0.0	1507	1510–1538	
	0.36	0.7	0.3	0.036	0.06	0.035	0.25	0.25	0.05	0.05	0.015	0.09	0.015	0.1	1493		
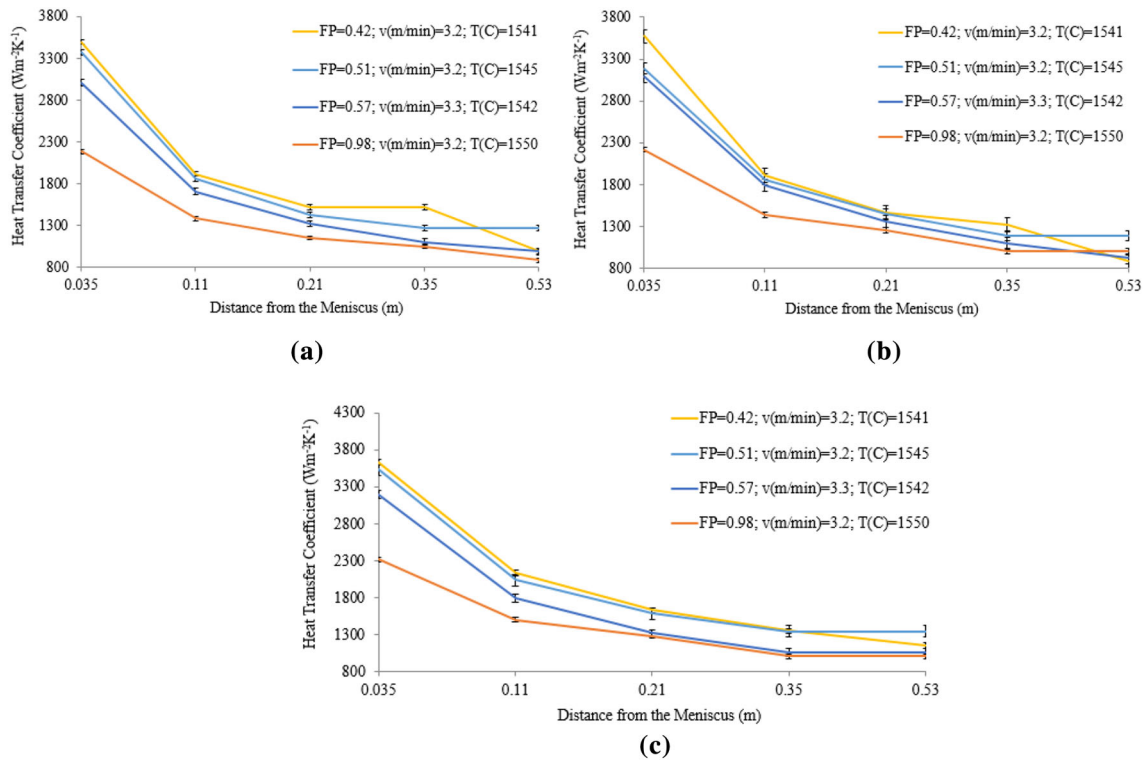
Fig. 3 Effect of chemical composition on heat transfer coefficient: **a** side face, **b** inner face, **c** outer face. All the results have the same casting speed of 3.2 m/min
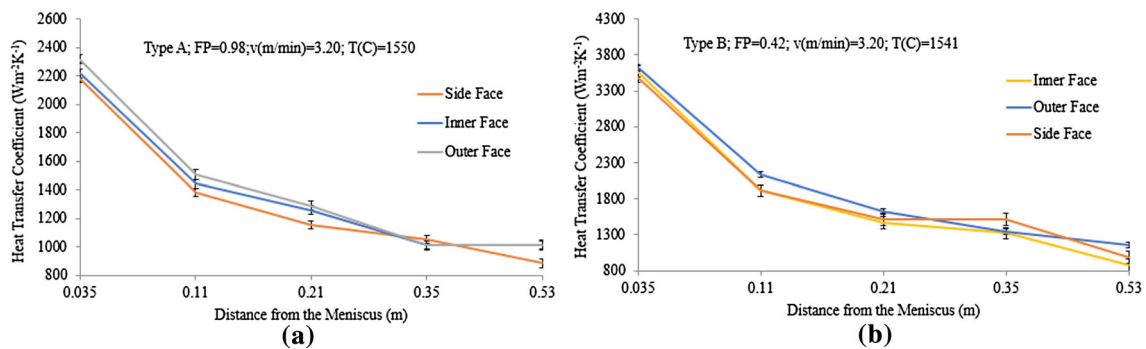

Fig. 4 Heat transfer coefficient at the three surfaces. **a** Steel type A, **b** steel type B
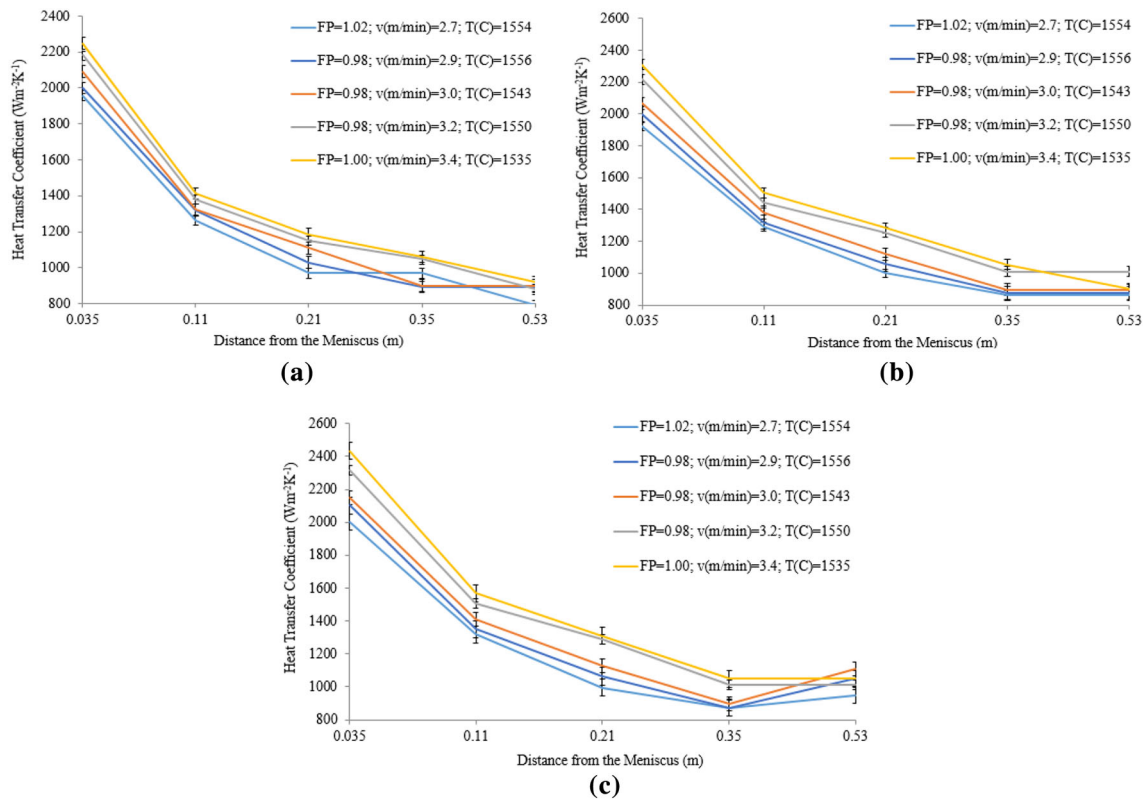
Fig. 5 Casting speed influence on the heat transfer coefficient for steel type A—**a** side face, **b** inner face, **c** outer face

flow. Finally, with less thermal contraction the metal/mold interface will have a better contact.

The effect of casting temperature is shown in Fig. 7. From this figure, it is possible to observe that the effect of the casting temperature does not affect the heat transfer coefficient, and hence can be neglected. Similar conclusions can be found [10, 37].

4.2 Analysis of the overall heat transfer coefficient

After obtaining the heat transfer coefficient, $h_{m/m}$, for all parameters shown in Tables 1 and 2, we evaluated the overall heat transfer coefficient that takes into account all thermal resistances from the cooling water to the center of the ingot (see Fig. 1). The profile along with the length of the mold for the overall coefficient resembles to the $h_{m/m}$ coefficient at each mold interface. This is an expected result since the $h_{m/m}$ coefficient is responsible for the largest thermal resistance. Based on the results, we proposed a correlation for the overall heat transfer coefficient for each face that is given by:

$$h_{\text{overall}} = C_0 + C_1^{ez(t)\left(-\frac{1}{c_2}\right)}, \qquad (16)$$

where $z(t)$ (m) is the distance from the meniscus in the casting direction, and the constants C_0, C_1, and C_2 are determined from the experimental data. The constants C_0, C_1, and C_2 are shown in Table 3. Using the adjusted coefficients, we present the overall heat transfer coefficients in Fig. 8 for side (Fig. 8a) and inner (Fig. 8b) faces, for several continuous casting parameters.

The average and maximum relative error between the curves obtained from Eq. (15) and experimental results is about 4 and 7%, respectively.

4.3 Numerical–experimental analysis of the heat transfer coefficient in the sprays and radiation/natural convection zones

Based on the procedure described at the end of Sect. 3, we estimated the heat transfer coefficient for each zone of sprays and for radiation/natural convection (tertiary) zone for all carbon steels investigated. The flow rates and the heat transfer coefficients for the spay regions and the heat transfer coefficient for tertiary region for all steels analyzed are presented in Table 4.
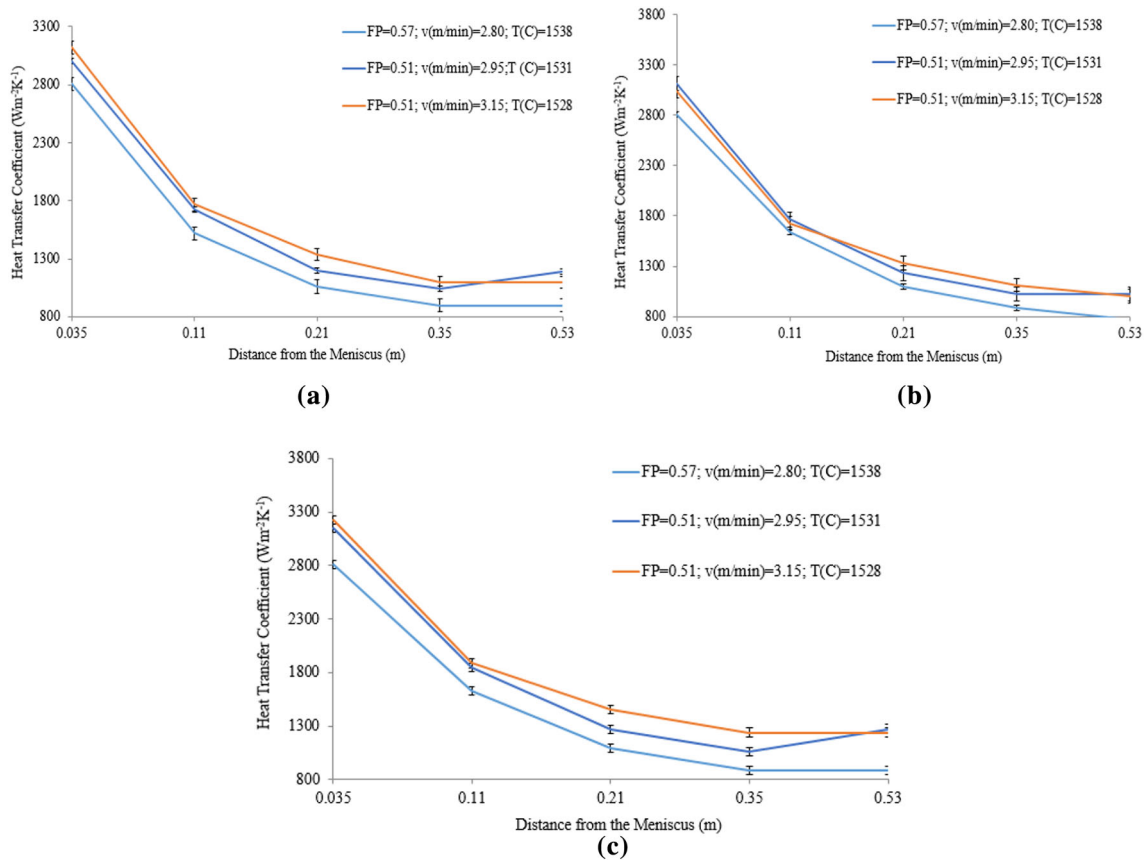
Fig. 6 Casting speed influence on the heat transfer coefficient for steel type B—**a** side face, **b** inner face, **c** outer face
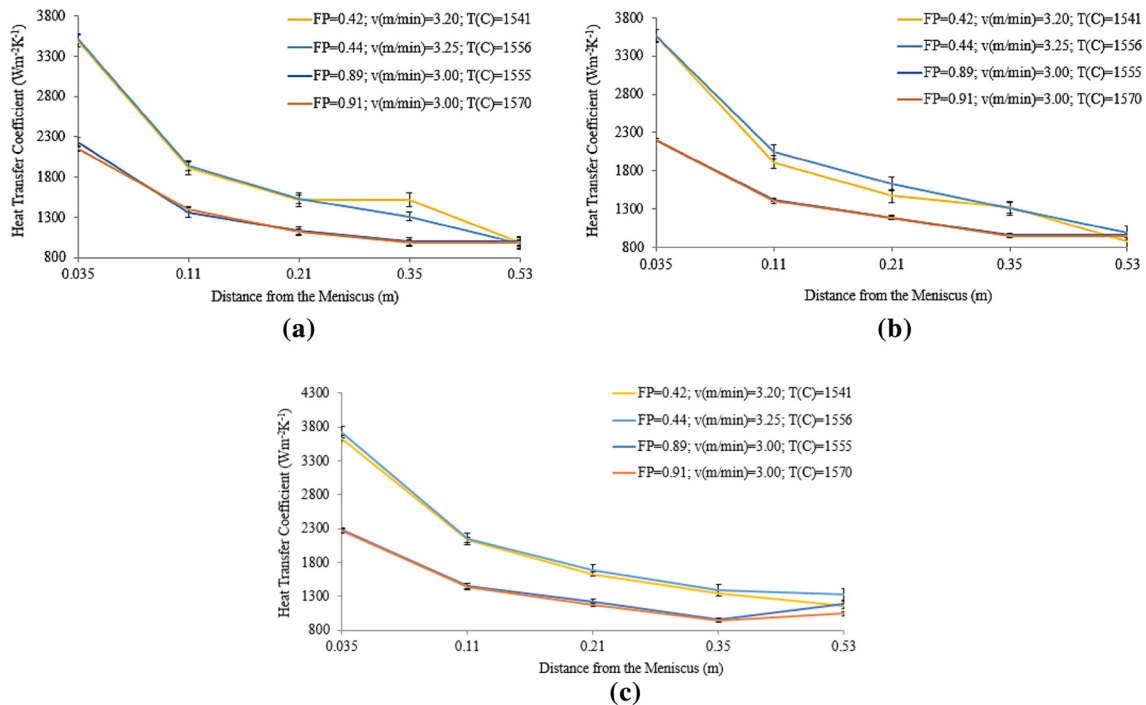

Fig. 7 Casting temperature influence on the heat transfer coefficient. **a** side face, **b** inner face, **c** outer face

Table 3 Constants of the overall heat transfer coefficient

	C_0	C_1	C_2
Outer	1652.549	0.076	1012.3554
Inner	1382.753	0.11003	892.5904
Side	323.349	0.10339	908.72076

5 Conclusions

In this work, the heat transfer behavior for a particular continuous casting process was studied using a numerical–experimental approach, IHCP, for all the three solidification stages (mold, secondary, and tertiary). This methodology provided satisfactory results since it could detect in the mold region the effect of the carbon content on the heat transfer coefficient for A and B steel types. Furthermore,

the highest values of the heat transfer coefficient were observed at the outer face of the mold for all investigated parameters. Such a behavior was expected due to the bending of the mold and weight of the ingot that help to reduce the thermal resistance. Experimental measurements assist in the calibration of the numerical heat transfer coefficient in distinct solidification regions, such as mold, sprays, and radiation/natural convection. In the mold region, we analyzed the heat transfer at the side, inner, and outer face of the metal/mold interface. In the spray zones, we adopted the heat transfer coefficient as dependent of the flow rate of the water and the number of sprays per zone. Finally, in the radiation/natural convection stage, we verified a single coefficient for each interface. We also proposed a correlation to evaluate the global coefficient that takes into account all simulated parameters for the different steel types.
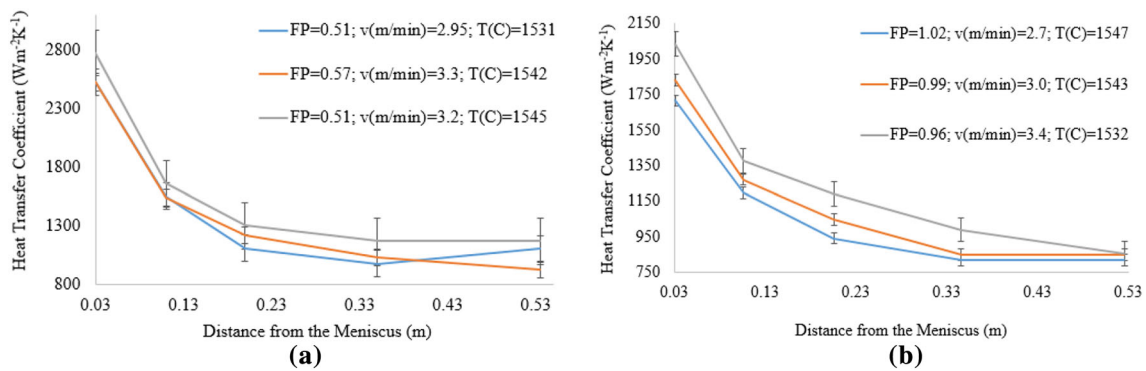

Fig. 8 The overall heat transfer coefficient—**a** side face, **b** inner face

Table 4 Water flow rates of and the convective heat transfer in the spays and radiation/natural convection zones

Steel grade	v_{cas}	Sprays zones								Natural convection h (W m^{-2} K^{-1})
		1st zone		2st zone		3st zone				
		m (l/s)	h (W m^{-2} K^{-1})	m (l/s)	h (W m^{-2} K^{-1})	m (l/s)	h (W m^{-2} K^{-1})			
1013	2.7	2.58	666	2.55	660	2.25	610			150
	3.0	2.87	711	2.83	705	2.5	652			147
	3.2	3.07	741	3.02	734	2.67	679			154
1028	2.7	2.23	574	2.2	569	1.95	532			157
	3.0	2.48	609	2.43	602	2.17	564			153
	3.2	2.65	632	2.6	625	2.32	586			148
1034	2.7	2.12	557	2.08	552	1.85	517			145
	3.0	2.35	591	2.32	586	2.05	547			153
	3.2	2.5	611	2.47	607	2.18	567			158

References

1. Santos CA, Spim JA, Garcia A (2003) Mathematical modeling and optimization strategies (genetic algorithm and knowledge base) applied to the continuous casting of steel. Eng Appl Artif Intell 16(5):511–527
2. Das SK (1999) Thermal modelling of DC continuous casting including submould boiling heat transfer. Appl Therm Eng 19(8):897–916
3. Saraswat R, Maijer DM, Lee PD, Mills KC (2007) The effect of mould flux properties on thermo-mechanical behaviour during billet continuous casting. ISIJ Int 47(1):95–104
4. Vynnycky M (2013) On the onset of air-gap formation in vertical continuous casting with superheat. Int J Mech Sci 73:69–76
5. Janik M, Dyja H, Berski S, Banaszek G (2004) Two-dimensional thermomechanical analysis of continuous casting process. J Mater Process Technol 153:578–582
6. Pinheiro CA, Samarasekera IV, Brimacomb JK, Walker BN (2000) Mould heat transfer and continuously cast billet quality with mould flux lubrication Part 1 Mould heat transfer. Ironmak Steelmak 27(1):37–54
7. Huang X, Thomas BG (1998) Modeling of transient flow phenomena in continuous casting of steel. Can Metall Q 37(3–4):197–212
8. Brimacombe JK, Samarasekera IV (1994) The challenge of thin slab casting. Iron Steelmak 21(11):29–39
9. Mizikar EA (1970) Spray-cooling investigation for continuous casting of billets and blooms. Iron Steel Eng 47(6):53–60
10. de Barcellos VK, Ferreira CR, Dos Santos CA, Spim JA (2013) Analysis of metal mould heat transfer coefficients during continuous casting of steel. Ironmak Steelmak 37(1):47–56
11. Pascon F, Habraken AM (2007) Finite element study of the effect of some local defects on the risk of transverse cracking in continuous casting of steel slabs. Comput Methods Appl Mech Eng 196(21):2285–2299
12. Wolf M, Kurz W (1981) The effect of carbon content on solidification of steel in the continuous casting mold. Metall Trans B 12(1):85–93
13. Garcia A, Prates M (1983) The application of a mathematical model to analyze ingot thermal behavior during continuous casting. In: Proceedings of the fourth IFAC symposium, vol 16, no 15. Helsinki, Finland, pp 273–279
14. Hills AW (1965) Simplified theoretical treatment for transfer of heat in continuous-casting machine moulds. J Iron Steel Inst 203:18
15. Cheung N, Garcia A (2001) The use of a heuristic search technique for the optimization of quality of steel billets produced by continuous casting. Eng Appl Artif Intell 14(2):229–238
16. Wang X, Kong L, Du F, Yao M, Zhang X, Ma H, Wang Z (2016) Mathematical modeling of thermal resistances of mold flux and air gap in continuous casting mold based on an inverse problem. ISIJ Int 56(5):803–811
17. Krishnan M, Sharma DG (1996) Determination of the interfacial heat transfer coefficient h in unidirectional heat flow by Beck's non linear estimation procedure. Int Commun Heat Mass Transf 23(2):203–214
18. Kumar TP, Prabhu KN (1991) Heat flux transients at the casting/chill interface during solidification of aluminum base alloys. Metall Trans B 22(5):717–727
19. Beck JV (1988) Combined parameter and function estimation in heat transfer with application to contact conductance. J Heat Transf 110(4b):1046–1058
20. Ho K, Pehlke RD (1985) Metal-mold interfacial heat transfer. Metall Trans B 16(3):585–594
21. Beck JV (1970) Nonlinear estimation applied to the nonlinear inverse heat conduction problem. Int J Heat Mass Transf 13(4):703–716
22. Maliska CR (2004) Heat transfer and computational fluid mechanics, Florianópolis, 2ª edn. Editora LTC. (**In Portuguese**)
23. Patankar SV. Numerical heat transfer and fluid flow: computational methods in mechanics and thermal science
24. Demirdžić I (2016) A fourth-order finite volume method for structural analysis. Appl Math Model 40(4):3104–3114
25. Filippini G, Maliska CR, Vaz M (2014) A physical perspective of the element-based finite volume method and FEM-Galerkin methods within the framework of the space of finite elements. Int J Numer Methods Eng 98(1):24–43
26. Vaz M, Muñoz-Rojas PA, Filippini G (2009) On the accuracy of nodal stress computation in plane elasticity using finite volumes and finite elements. Comput Struct 87(17):1044–1057
27. Marcondes F, Santos LO, Varavei A, Sepehrnoori K (2013) A 3D hybrid element-based finite-volume method for heterogeneous and anisotropic compositional reservoir simulation. J Petrol Sci Eng 31(108):342–351
28. Slone AK, Pericleous K, Bailey C, Cross M (2002) Dynamic fluid–structure interaction using finite volume unstructured mesh procedures. Comput Struct 80(5):371–390
29. Garcia A (2001) Solidificação: Fundamentos e Aplicações, editora da Unicamp. São Paulo, Brasil, pp 201–242
30. Spinelli JE, Tosetti JP, Santos CA, Spim JA, Garcia A (2004) Microstructure and solidification thermal parameters in thin strip continuous casting of a stainless steel. J Mater Process Technol 150(3):255–262
31. Monrad, Pelton, Gnielinski and Florenko (2003) Cia Europa Metalli, Manual Técnico v. único, pp 44–65
32. Bolle E, Moureau JC (1946) Sprays cooling of hot surfaces: a description of the dispersed phase and a parametric study of heat transfer results. Proc Two Phase Flows Heat Transf 101:1327–1346
33. Brimacombe JK, Samarasekera IV, Lait JE (1984) Continuous casting: heat flow, solidification and crack formation., vol 2. Iron and Steel Society of AIME
34. Mahapatra RB, Brimacombe JK, Samarasekera IV (1991) Mold behavior and its influence on quality in the continuous casting of steel slabs: part II. Mold heat transfer, mold flux behavior, formation of oscillation marks, longitudinal off-corner depressions, and subsurface cracks. Metall Trans B 22(6):875–888
35. Tiaden J (1999) Phase field simulations of the peritectic solidification of Fe–C. J Cryst Growth 198:1275–1280
36. Grill A, Brimacombe JK, Weinberg F (1976) Mathematical analysis of stresses in continuous casting of steel. Ironmak Steelmak 3(1):38–47
37. Chow C, Samarasekera IV, Walker BN, Lockhart G (2002) High speed continuous casting of steel billets: part 2: mould heat transfer and mould design. Ironmak Steelmak 29(1):61–69